Accepted Manuscript

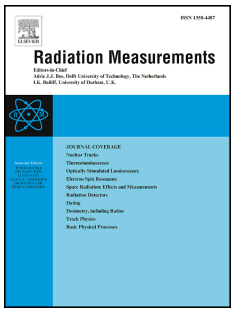

Optical determination of the width of the band-tail states, and the excited state and ground state energies of the principal dosimetric trap in feldspar

Svenja Riedesel, Georgina E. King, Amit Kumar Prasad, Raju Kumar, Adrian A. Finch, Mayank Jain

PII: S1350-4487(18)30371-8

DOI: 10.1016/j.radmeas.2018.08.019

Reference: RM 5986

To appear in: *Radiation Measurements*

Received Date: 26 May 2018

Revised Date: 31 August 2018

Accepted Date: 31 August 2018

Please cite this article as: Riedesel, S., King, G.E., Prasad, A.K., Kumar, R., Finch, A.A., Jain, M., Optical determination of the width of the band-tail states, and the excited state and ground state energies of the principal dosimetric trap in feldspar, *Radiation Measurements* (2018), doi: 10.1016/j.radmeas.2018.08.019.

Optical determination of the width of the band-tail states, and the excited state and ground state energies of the principal dosimetric trap in feldspar

Svenja Riedesel*[1,2], Georgina E. King[3], Amit Kumar Prasad[4,5], Raju Kumar[5], Adrian A. Finch[6], Mayank Jain[5]

[1] Department of Geography and Earth Sciences, Aberystwyth University, United Kingdom
[2] Institute of Geography, University of Cologne, Cologne, Germany
[3] Institute of Geological Sciences, University of Bern, Bern, Switzerland
[4] Schulich Faculty of Chemistry and Solid State Institute, Technion – Israel Institute of Technology, Haifa-32000, Israel
[5] Center for Nuclear Technologies, Technical University of Denmark, DTU Risø Campus, Roskilde, Denmark
[6] School of Earth and Environmental Sciences, University of St. Andrews, St. Andrews, United Kingdom

* Corresponding author:
Svenja Riedesel
Department of Geography and Earth Sciences
Aberystwyth University
Aberystwyth, Ceredigion
SY23 3DB
United Kingdom
riedeselsvenja@gmail.com

Abstract

We constrain parameters that determine thermal stability of the infrared stimulated luminescence (IRSL) signal in a suite of 13 compositionally different feldspar samples by optical probing. We focus specifically on the excited and ground state of the principal trap and the width of the sub-conduction band-tail states. Excitation spectra measured at room temperature result in approximate trap depth of about 2.04 eV and the excited state energy at 1.44 ± 0.02 eV, irrespective of feldspar composition for the sample's measured here. Fitting the non-resonant rising continuum of the excitation spectra suggests that the width of the band-tail states accessible from the ground state of the trap (ΔE) ranges from 0.21 to

0.47 eV at room temperature between the different samples. Photoluminescence measurements are used to constrain the full sub-conduction band-tail width (Urbach width, E_u) using the excitation-energy-dependent emission (EDE), resulting in values ranging from 0.26 to 0.81 eV. While the depth of the principal trap and its main excited state seem to be independent of feldspar composition, the difference between ΔE and E_u seems to be related to sample K-content.

Keywords

Trap depth; IR resonance; band-tail states; excitation spectrum; emission spectrum; excitation-energy-dependent emission

1 Introduction

Feldspar is widely used as a chronometer in luminescence dating. The development of post-infrared infrared-stimulated luminescence (post-IR IRSL) protocols (Thomsen et al., 2008; Thiel et al., 2011; Buylaert et al., 2012), which reduce the effects of athermal signal loss (anomalous fading, Wintle, 1973) have increased the use of feldspar in many luminescence studies. Whilst anomalous fading still poses a challenge for some samples, the infrared-stimulated luminescence (IRSL) of feldspar offers a number of advantages over quartz optically stimulated luminescence (OSL), including higher signal sensitivity and saturation dose. Furthermore, the newly developed infrared-photoluminescence (IR-PL) method (Prasad et al., 2017) can be used to date feldspar non-destructively, i.e. without depleting the trapped electron population, opening a range of new research opportunities. The recent methodological developments in feldspar luminescence dating have been paired with an increased understanding of luminescence recombination processes within feldspar

57 minerals (e.g. Jain and Ankjærgaard, 2011) and several models have been developed to
58 describe the thermal stability of feldspar IRSL (e.g. Jain et al., 2012; 2015; Li and Li, 2013;
59 Guralnik et al., 2015; Lambert et al., In Review).

60 In luminescence dating applications, provided that the specific luminescence signal
61 under investigation is sufficiently stable relative to the timescale being dated (Aitken, 1985),
62 exact knowledge of the kinetic parameters that govern the signal's stability is not necessary.
63 However, luminescence is increasingly being used to determine rock thermal histories (e.g.
64 Guralnik et al., 2015; King et al., 2016) and such applications require accurate constraint of
65 the parameters that govern thermal decay, in order to extrapolate the cooling history of
66 bedrock over geological timescales. Such extrapolations potentially result in the introduction
67 of large uncertainties on past rock temperatures (Yukihara et al., In Press). Requirement of
68 specialised instrumentation has meant that comparatively few studies have sought to
69 directly characterise the key physical parameters associated with feldspar lRSL thermal
70 decay. The focus of this study is to use optical methods to determine (i) the trap depth and
71 (ii) the excited state energy of the principal trap, and (iii) the width of the sub-conduction
72 band-tail states, in a suite of feldspar samples of different chemical compositions. Analysing
73 a range of different feldspars may provide insights into the cause of the differing thermal
74 stability observed between feldspars that are chemically different (e.g. Tsukamoto et al.,
75 2012).

76

77 **2 Previous investigations of luminescence kinetics of feldspar**

78 Feldspars are wide band-gap (~7.7 eV) alumino-silicates (Malins et al., 2004), and
79 defects in their crystal lattice allow storage, transport and recombination of charge carriers
80 (Fig. 1). Electrons get trapped in defects (trapping centres) following excitation by ionising

radiation. These trapping centres are able to store electrons over geological time, making trapped-charge dating techniques (luminescence and electron spin resonance dating) possible (Krbetschek et al., 1997; Ikeya, 1993). Electrons can be released from a trap when they receive sufficient energy, either from optical and/or thermal excitation (e.g. Aitken, 1985; Huntley et al., 1985) and when the released electron recombines with a hole (luminescence centre), a luminescence signal is produced (Fig. 1). The thermal stability of a luminescence signal, and thus its validity as a chronometer is at least partly determined by the electron trap depth of the signal under investigation.

2.1 The ground and excited state of the IRSL (principal) trap

Constraining the depth of the principal trap infeldspar has been the subject of fundamental research since the mid-1980s (e.g. Stickertsson, 1985; Hütt et al., 1988) however the exact defect associated with feldspar IRSL remains unclear. Initial research focussed on defining optimal stimulation and emission-detection wavelengths for sediment dating applications (e.g. Hütt et al., 1988; Bailiff and Poolton, 1991; Krbetschek et al., 1996; summary given in Krbetschek et al., 1997) whilst more recent studies have sought to identify the trap depth using the relationship between thermoluminescence (TL) emission peaks and IRSL signals (e.g. Murray et al., 2009; Tsukamoto et al., 2012), or isothermal holding experiments coupled with numerical models (e.g. Guralnik et al., 2015). It has been widely debated whether the luminescence of feldspar is derived from a single trap or multiple traps (e.g. Clark & Sanderson, 1994; McKeever et al., 1997; Baril & Huntley, 2003; Murray et al., 2009; Jain and Ankjærgaard, 2011), although spectroscopic evidence suggests that the same electron trapping centre participates in IRSL and post-IR IRSL signals (Andersen et al., 2012).

The trap depth (with respect to the edge of the conduction band) of a charge trapping centre is determined from the energy required to ionise it. The thermal activation energy required to evict charge from a trap is typically lower (e.g. Stickertsson, 1985; Hütt et al., 1988; Brown and Rhodes, 2017) than the optical energy (e.g. Kars et al., 2013). Hütt et al. (1988) initially constrained the optical activation energy required to release electrons from traps in feldspar, and thus the optical trap depth. They recorded a rising continuum (continuous increase in emission intensity with increasing excitation energy) in the excitation spectra of an irradiated microcline until ~2.25 eV, where their curves peaked (note that the following decrease in signal intensity reported in that study is an instrumental artefact). Poolton et al. (2002a, b) estimated the optical trap depths of $NaAlSi_3O_8$ and $KAlSi_3O_8$ as 1.97 eV and 1.99 eV, respectively, assuming a hydrogenic model, and validated their results against the experimental data of Bailiff and Poolton (1991) and Spooner (1994). Based on the thermal dependence of time-resolved (TR) green-light stimulated luminescence, Jain and Ankjærgaard (2011) argued that the trap depth of their orthoclase sample was likely to be >2.4 eV (see green arrow in Fig. 1A). Most recently Kars et al. (2013) determined the optical trap depths of $NaAlSi_3O_8$ (2.1 eV) and $KAlSi_3O_8$ (≥2.5 eV) by fitting excitation spectra measured at 10 K following Bøtter-Jensen et al. (2003).

The excited state energy of the principal trap can also be inferred from excitation spectra. Feldspar show a resonance peak at ~1.45 eV (e.g. Hütt et al., 1988; Baril and Huntley, 2003), with reported full width at half maximum (FWHM) values of 0.12 to 0.13 eV (Godfrey-Smith and Cada, 1996) and 0.11 to 0.21 eV (Baril and Huntley, 2003). Some studies have reported multiple IR excitation peaks (e.g. Hütt et al., 1988; Bailiff and Poolton, 1991; Clark and Sanderson, 1994) and Bøtter-Jensen et al. (1994) observed composition dependent

variations in the shape and position of the resonance peak for plagioclase, albite and potassium-rich feldspar.

2.2 Sub-conduction band-tail states

Whilst IR (~1.4 eV) stimulation excites electrons from the ground state to the excited state, it is insufficient for electrons to access the conduction band directly. Poolton et al. (2002a, b) suggested that sub-conduction band-tail states are present within feldspar (Fig. 1A, B), and that they play a key role in electron-hole recombination processes. Band-tail states arise due to imperfections and are distributed in energy levels above the valence band and below the conduction band. Charge in the band-tail states can migrate by hopping (e.g. Morthekai et al. 2012).

Poolton et al. (2009) used photo-transferred OSL (synchrotron photons of energies of 5.5 to 9.0 eV) measured at 10 K to determine the full sub-conduction band-tail width (i.e. Urbach width, E_u) for a $NaAlSi_3O_8$ (R27) and $KAlSi_3O_8$ (R28) sample, obtaining values of 0.28 eV and 0.67 eV respectively. Fitting of energy-resolved stimulation spectra of the same samples (measured at 10 K), but after x-ray irradiation yielded values of 0.32 eV ($NaAlSi_3O_8$, R27) and 0.54 eV ($KAlSi_3O_8$, R28). Poolton et al. (2009) also determined the width of the band-tail states, which are accessible from the ground state of the defect (referred to as ΔE), by fitting the non-resonant rising continuum excitation spectrum of the same samples at 300, 200, 100 and 10 K. They found a decrease in ΔE at lower temperatures (from 0.12 to 0.09 eV for $NaAlSi_3O_8$ and from 0.30 to 0.16 eV for $KAlSi_3O_8$). Based on this, Poolton et al. (2009) identified two different, temperature dependent, processes governing IRSL in feldspar: (i) a thermally assisted hopping process at temperatures >100 K, and (ii) an athermal process, which disables hopping, although tunnelling remains possible (either via tail-to tail, or tail-to-

recombination centre). Whilst at temperatures > 100 K (i.e. with thermal assistance) a large proportion of band-tail states are accessed resulting in a large ΔE, at temperatures < 100 K, ΔE is comparably small and invariant with temperature. Kars et al. (2013) used the same approach to determine ΔE for the same samples examined by Poolton et al. (2009) and calculated values of 0.18 (R27) and 0.23 eV (R28) for measurements made at 10 K.

More recently Prasad et al. (2016) developed a new method of determining the Urbach width (i.e. the width of the sub-conduction band-tail states, referred to as E_u). Using a photoluminescence (PL) emission in the green-orange, they observed an excitation-energy-dependent emission (EDE). The emission peak position shifted linearly, while the peak intensity varied exponentially with a change in the excitation energy; this effect was attributed to the exponentially distributed density of the sub-conduction band-tail states. High excitation energies are able to access band-tail states closer to the conduction band edge, where the density of states is highest and emission intensities are correspondingly larger. Further from the conduction band edge, the density of states is lower and excitation to this part of the band-tail (i.e. using a lower energy excitation) results in a lower emission intensity. Repeating the experiment at 7, 100 and 295 K yielded PL emission spectra that were broadly similar, supporting the hypothesis that the emissions reflect a continuous distribution of the band-tail states. Using this approach, Prasad et al. (2016) obtained E_u of 0.32 eV for the oligoclase sample investigated. Prasad and Jain (2018) present and discuss a detailed model of the EDE and its application for measuring the band-tail width. Their measurements at 295 K resulted in E_u values of 0.29 to 0.51 eV. EDE at cryogenic temperatures (7 K) and room temperature (295 K) yielded similar results for their perthitic sample (R58) of 0.33 eV. However, R28 exhibited different band-tail widths at different measurement temperatures: 0.29 eV (295 K) compared to 0.41 eV (7 K). Prasad and Jain

(2018) attribute these differences to an increase in retrapping efficiency, from the lower band-tail states at cryogenic temperatures, related to mobility, which is a function of the net density of states.

As is clear from the discussion above, while there are several articles characterising the excited state energy of the principal trap, only few studies have reported the trap depth and the band tail width. In this contribution, our focus is to characterise the ground and excited state energies of the principal trap and the width of the band tail states using optical methods, in feldspars of different chemical compositions. Specifically, we use excitation spectra to explore (i) the excited and ground state of the IRSL trap and (ii) use the approach of Poolton et al. (2009) and Kars et al. (2013) to fit the rising continuum of the same spectra to indirectly estimate the trap depth and the sub-conduction band-tail states accessible from the ground state of the trap (ΔE). Finally, (iii) following Prasad et al. (2016) and Prasad and Jain (2018), we use EDE to directly measure the width of the sub-conduction band-tail states (i.e. the Urbach width, E_u). Characterising the energy levels of the principal trap and the width of the band tail states is necessary for understanding the thermal stability of IRSL in different feldspar samples.

3 Material and methods

3.1 Samples

The suite of feldspars selected for this study are summarised in Table 1 and Figure 2. Through characterising samples with different chemical compositions, we can contrast the kinetic parameters of different feldspar with chemical control. We investigated five museum specimens, two sediment samples from Japan (Riedesel et al., 2018, for JSH1-13), and seven bedrock samples from the KTB borehole in Germany, the Japanese Alps, Namche Barwa in

the Himalaya, and the Mont Blanc massif, some of which have been studied previously (Guralnik et al., 2015; King et al., 2016; Lambert et al., In Review). The majority of the samples are part of the alkali feldspar solid solution, although one is an alkali feldspar end-member (Cleavelandite), one is a ternary feldspar (KTB-383-C) and one (DK4) is a plagioclase. Only phase-pure K-feldspar is stable at low (<300 °C) temperature and hence we assume that the alkali feldspars are perthites, comprising intergrowths of K-feldspar (either orthoclase or intermediate microcline) and intermediate albite. One sample, R1-11A, is a microcline cryptoperthite in which the K- and Na-feldspars are coherently intergrown on nm-scales and in which the interfaces between the two phases comprise a significant proportion of the volume of the mineral. F1 is an International Atomic Energy Agency (IAEA AQCS) secondary reference feldspar (IAEA, 1999).

3.2 Instrumentation

Measurements were made using the Risø station for CryOgenic Luminescence Research (COLUR; Prasad et al., 2016, 2017), at the Centre for Nuclear Technology, Technical University of Denmark, Risø Campus, Roskilde, Denmark. The measurements were made using a Tungsten halogen lamp, for excitation between 500 and 1000 nm, and a CW Xenon lamp for excitation between 370 and 560 nm. Excitation wavelengths were selected using a double-grating Czerny-Turner monochromator and excitation spectra were recorded through a U340 filter with a UV-sensitive photomultiplier tube (PMT). Emission spectra were detected using the UV-sensitive PMT together with the monochromator. All spectra were corrected for excitation light flux and system response; excitation spectra were converted into photons/s/unit energy interval. Sample material was mounted on the sample holder within COLUR using carbon tape. The sample holder of COLUR comprises the cold finger of a

closed loop He-cryostat that allows temperature dependent measurements to be performed. A blank aliquot of carbon tape was measured at 300 K to quantify any background signal.

3.3 Excitation spectra: Determining trap depth, band-tail width and the excited state of the IRSL (principal) trap

A large aliquot of sand-sized sample material or a single crystal (~2 mm diameter, < 1 mm thick, sample dependent, see Table 1) were beta irradiated to deposit 500 Gy using a Sr^{90}/Y^{90} beta source attached to a Risø TL/OSL Reader (TL-DA-20). Prior to mounting in the COLUR sample chamber, the samples were preheated for 60 s at 250 °C to remove trapped charge which is thermally unstable over laboratory timescales. Excitation spectra were measured from 500 to 1000 nm, using a step size of 5 nm, a bandpass of 10 nm and an integration time of 1 s. We tested the effect of measurement temperature on selected sample F1, which was measured at 7 K and 300 K; all other measurements were made at 300 K.

3.4 Emission spectra: Determining the band-tail width using the excitation-energy-dependent emission (EDE)

The width of the full sub-conduction band-tail states (E_u) of the different samples were determined following Prasad et al. (2016), using fresh, non-irradiated large aliquots of sand-sized samples or single crystals (~2 mm diameter). Samples were mounted on the sample holder in the measurement chamber and excited from 370 to 520 nm using 5, 10 or 20 nm steps, dependent on samples brightness. Emission spectra were recorded with a 1 nm wavelength-scanning interval in the range of 390 to 540 nm, using a 2 nm bandpass. The integration time was either 1 or 10 s, depending on sample brightness. At least two

248 measurements were repeated for each sample within each measurement cycle to confirm
249 measurement reproducibility, and two samples (NB120 and MBT-I-2430) were measured
250 twice. The results of these repeat measurements were consistent with each other.
251
252 **4 Results**
253 **4.1 Excitation spectra: Determining trap depth, accessible band-tail width and the excited**
254 **state of the IRSL trap**
255 The carbon tape substrate (blank measurement) had no detectable emission at any
256 excitation wavelength. The excitation spectrum of each sample showed two distinct features
257 (see examples in Fig. 3B); a resonance peak centred at ~1.45 eV in the low energy region
258 (1.24 to 1.70 eV), followed by a monotonic rise to the maximum excitation energy of 2.48 eV
259 measured here. These results are qualitatively consistent with previous studies (e.g., Baril
260 and Huntley, 2003).
261 The luminescence intensities and the contrast between the two features vary
262 between the different samples (Fig. 3A, B, Figs. S-4-S-7). Cleavelandite (albite) shows the
263 brightest signal intensity whereas plagioclase sample DK4 has very dim luminescence. For all
264 samples except Cleavelandite, F1 and KTB-383-C, the resonant luminescence emission
265 intensity is stronger than that at the highest excitation energy. In addition to the IR
266 resonance peak, MBT-I-2430 shows a broad absorption peak centred at ~2.1 eV, which is
267 superimposed on the rising continuum (Fig. 3B).
268 F1 was measured at 300 and 7 K (Fig. 3A), to investigate the effect of different
269 measurement temperatures. The initial luminescence intensity in response to excitation of
270 2.25 eV is about an order of magnitude greater at room temperature, relative to

measurement at 7 K, which is significant as some of our samples showed very weak luminescence. The IR resonance peak is absent in the 7 K excitation spectrum (Fig. 3A).

4.1.1 Trap depth

Following Kars et al. (2013) we fitted part of the rising continuum present in the excitation spectra of Cleavelandite, KTB-383-C, NB139, NB120, MBT-F-5704, MBT-I-2430, R1-11A, JSH1-13 and HAM-5 to estimate trap depth using equation [1] (Bøtter-Jensen et al., 2003); the excitation spectra of the other samples were not sufficiently bright.

$$\sigma(E, Et) \propto \frac{(E-E_t)^{\frac{3}{2}}}{E(E-E_t(1-\frac{m_0}{m*}))} \quad [1]$$

where σ is the photo-ionisation cross-section, E the excitation energy (eV), E_t the trap depth (eV), $m*$ the effective electron mass (fixed at m* = 0.79 m_0, Poolton et al., 2001; Kars et al., 2013) and m_0 the electron rest mass. Data were fitted in MATLAB and following Kars et al. (2013), only a part of the rising continuum was fitted (Fig. 4, S-1, -2 and -3), using equation 1 we fitted the luminescence emission intensity for each excitation energy (E). Kars et al. (2013) measured excitation spectra up to 2.80 eV, however due to instrumental limitations during the analytical period, the maximum excitation energy explored in this study was 2.48 eV. We tested the influence of fitting different excitation energy ranges on the obtained E_t to evaluate whether our spectra are sufficiently described (i.e. from 2.10 eV to 2.35 eV in 0.05 eV steps, Table S-1). We recorded an average variance of 7 %, with a trend towards higher E_t values as the lowest fitted excitation energy increased.

We report values derived from fitting the emission intensity for excitation energies ranging from 2.30 to 2.48 eV and the mean optical trap depth is 2.04 ± 0.05 eV. Sample

MBT-I-2430 exhibit the greatest trap depths of 2.15 ± 0.01 and Cleavelandite has the shallowest trap depth of 1.99 ± 0.01 eV (Table 2). Given that the high-energy plateau predicted by equation 1 is not observed in our experimental data, the model fits are mathematically poorly constrained and these trap depths should be considered as preliminary estimates.

4.1.2 Excited state of the IRSL trap

The IR resonance peak was fitted with a single Gaussian distribution [eq. 2] to characterise the excited state of the IRSL trap.

$$f(E) = k * exp\left(-\frac{1}{2} * \frac{(E-\mu)^2}{\sigma^2}\right) \quad [2]$$

where *k* is a pre-exponential factor, *E* the corresponding excitation energy, μ the mean energy of the Gaussian distribution and σ the standard deviation. All samples showed similar IR resonance with the Gaussian distribution centred between 1.41 and 1.46 eV (Fig. 3, Figs. S-4, S-5). The FWHM varied from 0.16 to 0.40 eV; results are given in Table 2.

4.1.3 Estimation of band-tail width

To obtain the width of the band-tail states (ΔE) accessible from the ground state of the trap, following Kars et al. (2013) we fitted the rising continuum from 1.80 to 2.48 eV with equation 3 (Poolton et al., 2009).

$$OSL(E) \propto exp\left(\frac{E-E_t}{\Delta E}\right) \quad [3]$$

where E is the excitation energy, E_t the trap depth and ΔE the band-tail width accessible from the ground state of the trap. The broad absorption peak at ~2.1 eV superimposed on the rising continuum of sample MBT-I-2430 (Fig. 3B, Fig. S-3C) was excluded from the fit of this sample, so that the final excitation energy range considered was limited to 2.22 to 2.48 eV.

The quality of fit varied between samples. It was not possible to calculate ΔE for KRG-16-112 or DK4, and some deviation between the fit and the measured data is recorded for Cleavelandite, JSH1-13, HAM-5 and KTB-383-C in the low excitation energy region (Figs S-6 and S-7). Calculated ΔE ranges from 0.22 eV (MBT-I-2430) to 0.47 eV (NB120). Compared to the overall range in ΔE, measurements of F1 at 300 K (0.29 eV) and 7 K (0.21 eV) yield similar values.

4.2 Estimation of band-tail width using the excitation-energy-dependent emission (EDE)

The PL emission spectra of the different samples were similar and are characterised by a single emission peak. Reducing the excitation energy systematically causes signal intensities to decrease and the emission peak to become narrower and to shift to lower emission energy. At ~2.2 eV excitation, no detectable peak is observed. The area under the PL peak was integrated and an exponential relationship between the PL intensity (integrated PL peak area) and the corresponding excitation energy was observed (Fig. 5; Figs. S-8, S-9). Taking the natural logarithm of the integrated PL peak area enabled us to fit a linear regression between ln(PL) and the excitation energy (Fig. 5). The inverse of the slope of the fitted line represents the band-tail width. Based on this relationship and following the approach of Prasad et al. (2016) we estimated E_u for all samples by calculating the inverse of the slope. This resulted in band-tail width estimates ranging from 0.26 to 0.81 eV for

plagioclase sample DK4 and ternary feldspar sample KTB-383-C respectively, full results are listed in Table 2. No shift in peak position was observed for sample R1-11A making it impossible to determine E_u for this sample.

5 Discussion

Previous studies have indicated that the thermal stability of different feldspars may vary (e.g. Tsukamoto et al., 2012). However, no dependence of either the energy of the trap depth or the excited state of the principal trap are apparent for the feldspars investigated here (Fig. 7). The IR resonance of our samples is in agreement with published values (Baril and Huntley, 2003; Poolton et al., 2009) and has an average peak position of 1.44 ± 0.02 eV and FWHM of 0.19 to 0.40 eV. Bøtter-Jensen et al. (1994) proposed that alkali-feldspar chemical composition influences the IR-resonance. However, no clear relationship between mode IR resonance or FWHM, and sample chemical composition, is apparent for our data (Fig. 7).

The similarity between the different feldspar variants indicates that the defect causing IR absorption is likely to be on the feldspar silicate framework, rather than a substitution or defect on the metal site (the compositions and symmetry of which changes substantially across the feldspar mineral group), which is in agreement with previous work (e.g. Short, 2004). However, a specific defect has not yet been associated with IR absorption in feldspar.

The trap depth is a critical parameter for determining the thermal stability. To illustrate, assuming first order kinetic behaviour (which is rarely the case, cf. Guralnik et al., 2015), an E_t of 2.0 eV yields a lifetime at 50 °C of 13 Ga whereas an E_t of 1.90 eV yields a lifetime of only 359 Ma assuming a lattice vibration frequency factor (s) of $3.9 \times 10^{13}\ s^{-1}$. In

feldspar, the band-tail width also modifies thermal stability (e.g. Li and Li, 2013) and constraining the trap depth of feldspar is challenging because of the presence of the band-tail states (Poolton et al., 2009; Kars et al., 2013). However, despite this it is encouraging that all of our samples, irrespective of chemical composition, yield a nominal average optical trap depth of 2.04 eV with a relatively small standard deviation of 0.05 eV. Furthermore the individual estimates of trap depth are within uncertainties of one another (Figure. 7; Table 2). These preliminary data suggest that the defect or defects interrogated in the optical probing experiments presented here are part of the feldspar alumino-silicate framework, which is broadly consistent between all feldspar variants. In terms of trap depth calculations, a common value of E_t may be applicable to feldspar of different compositions, and further investigations using low temperature OSL excitation spectra, and/or newly developed optical probing methods to directly characterise the IRSL trap depth without the effects of competing recombination processes (Prasad et al., 2017), will be useful to investigate this potential in the future.

Regarding the width of the sub-conduction band-tail states, both methods, viz. the excitation spectra measured at 300 K to determine ΔE (equation 3) and EDE (Prasad et al., 2016; Prasad and Jain, 2018) used to determine E_u yield broadly similar results for some samples (Fig. 6). ΔE ranged from 0.21 to 0.46 eV and E_u from 0.26 to 0.81 eV (Figs. 6, 7). These results are within the range of previously published values (Poolton et al., 2009; Prasad and Jain, 2018). The reference feldspars that we investigated (F1, Cleavelandite and DK4; listed from medium to low potassium content), exhibit a decrease in E_u with reducing K-content from 0.48 ± 0.03 eV (orthoclase content: 61.3%) to 0.26 ± 0.02 eV (orthoclase component: 0.5 %). However, this trend is not apparent in the non-reference feldspar samples measured as large aliquots of sand-sized material, which may be a consequence of

signal averaging across grains of different chemical composition. Single-phase feldspars are unlikely in this sand-sized material, and the feldspars under investigation are likely to comprise intergrowths of K-feldspar and Na-feldspar. Consequently the apparent consistency might be related to one phase dominating the response in these experiments.

The relationship between E_u and ΔE is also interesting (Figure 6). Our results suggest that ΔE is either consistent with E_u (five samples) or smaller than E_u (five samples). This relationship confirms expectation because whereas E_u (the Urbach band-tail width) mainly maps the excitation efficiency, ΔE (the width of the band-tail accessible from the ground state of the trap) depends on both the excitation efficiency and the recombination efficiency, which in turn is a function of the energy of the band tail state (Jain and Ankjærgaard, 2011) and temperature. Interestingly four out of five samples with $\Delta E < E_u$ have relatively low K contents (F1, JSH1-13, HAM-5, KTB-383-C), potentially indicating reduced recombination efficiency with band-tail energy in K-poor feldspars. Poolton et al. (2009) and Kars et al. (2013) also found that ΔE is narrower in $NaAlSi_3O_8$ than in $KAlSi_3O_8$, providing support for this observation.

Whilst it is important to consider the absolute width of the band-tail states, the absolute density of band-tail states will also impact the thermal stability of luminescence signals in feldspars. This aspect has not been investigated in the present study but should be considered for assessing thermal stability of IRSL.

6 Conclusion

In this study we investigated the kinetic parameters of feldspar that are thought to determine thermal decay using optical probing, and attempted to relate these parameters to feldspar chemical composition. We obtained a nominal average estimate for the optical trap

depth of 2.04 ± 0.05 eV and the energy of the excited state of the IRSL trap of 1.44 ± 0.02 eV, with FWHM ranging from 0.16 to 0.40 eV. Detailed analyses of both the full sub-conduction band-tail width (E_u) and the sub-conduction band-tail states accessible from the ground state of the trap (ΔE), revealed values ranging from 0.2 to 0.8 eV. All values are consistent with previous studies. Interestingly the difference between ΔE and E_u is greater for samples with low K-content, potentially indicating that recombination efficiency must vary more with band tail energy in K poor feldspars. Based on these findings we tentatively conclude that the defect or the defects leading to IRSL in feldspar are within the alumino-silicate framework of feldspar, which is almost the same for all alkali feldspars and would explain the similarity in our results. In contrast to the trap energy levels (ground and excited state), ΔE, E_u and the FWHM of the excited state exhibited larger variability between samples; combining these data with numerical models of feldspar thermal decay, and contrasting them with isothermal decay data in future work will provide further insights into which parameters are the key drivers of differences in the thermal stability of feldspars.

Acknowledgements

SR performed the measurements during her M.Sc., which was financially supported by the *Deutschlandstipendium* of the *Bundesministerium für Bildung und Forschung – Stiftung Studium und Lehre* (Ministry for Education and Research of the German government). The paper was written, during SR's PhD, which is financed by an *AberDoc PhD Scholarship* of Aberystwyth University. An *Erasmus+ student mobility grant* enabled SR's research stay at the Center for Nuclear Technologies, Technical University of Denmark, DTU Risø Campus, Roskilde, Denmark. GEK acknowledges support from SNSF grant number PZ00P2_167960.

Samples HAM-5 and JSH1-13 were taken in the framework of the QuakeRecNankai project, funded by the Belgian Science Policy Office (BELSPO BRAIN-be BR/121/A2). We thank Benny Guralnik for the provision of KTB-383-C, Renske Lambert for MBT-I-2430 and MBT-F-5704, Javier Garcia-Guinea for Cleavelandite and David Sanderson for F1.

We thank two anonymous reviewers for their constructive comments that helped to improve the manuscript.

445 **References**

446 Aitken, M. J., 1985. Thermoluminescence dating. Oxford, Academic Press, 385 p.

447 Andersen, M. T., Jain, M., Tidemand-Lichtenberg, P., 2012. Red-IR stimulated luminescence
448 in K-feldspar: Single or multiple trap origin? J. Appl. Phys. 112, 1–11.

449 Bailiff, I. K., Poolton, N. R. J., 1991. Studies of charge transfer mechanisms in feldspars. Nucl.
450 Tracks. Radiat. Meas. 18, 111–118.

451 Baril, M. R., Huntley, D. J., 2003. Optical excitation spectra of trapped electrons in irradiated
452 feldspars. J. Phys.: Condens. Matter 15, 8011–8027.

453 Bøtter-Jensen, L., McKeever, S. W. S., Wintle, A. G., 2003. Optically Stimulated Luminescence
454 Dosimetry. Elsevier, Amsterdam, 375 p.

455 Bøtter-Jensen, L., Duller, G. A. T., Poolton, N. R. J., 1994. Excitation and emission
456 spectrometry of stimulated luminescence from quartz and feldspars. Radiat. Meas. 23
457 (2/3), 613–616.

458 Brown, N. D., Rhodes, E. J., 2017. Thermoluminescence measurements of trap depth in alkali
459 feldspars extracted from bedrock samples. Radiat. Meas. 96, 53–61.

460 Burg, J.-P., Davy, P., Nievergelt, P., Oberli, F., Seward, D., Diao, Z., Meier, M., 1997.
461 Exhumation during crustal folding in the Namche-Barwa syntaxis. Terra Nova 9, 53-56.

462 Bussy, F., Schaeltegger, U., Marro, C., 1989. The age of the Mont Blanc granite (western
463 Apls): A heterogenous isotopic system dated by Rb-Sr whole rock determination on its
464 microgranular enclaves. Schweiz. Mineral. Petror. Mitt. 69, 3-13.

465 Bussy, F., Von Raumer, J. F., 1993. U-Pb dating of Palaeozoic events in the Mont-Blanc
466 crystalline massif, western Alps. Terra Nova Abstr. 5, 382.

467 Buylaert, J.-P., Jain, M., Murray, A. S., Thomsen, K. J. Thiel, C., Sohbati, R., 2012. A robust
468 feldspar luminescence dating method for Middle and Late Pleistocene sediments.
469 Boreas 41, 435–451.

470 Cassedanna, J. P., Roditi, M., 1996. The location, geology and mineralogy of gem tourmalines
471 in Brazil. J. Gemm. 25, 263-298.

472 Clark, R.J., Sanderson, D.C.W., 1994. Photostimulated luminescence excitation of
473 spectroscopy of feldspars and micas. Radiat. Meas. 23, 641–646.

474 Godfrey-Smith, D. I., Cada, M., 1996. IR stimulation spectroscopy of plagioclase and
475 potassium feldspars, and quartz. Radiat. Prot. Dos. 66, 379–385.

476 Guralnik, B., Jain, M., Herman, F., Ankjærgaard, C., Murray, A. S., Valla, P. G., Preusser, F.,
477 King, G. E., Chen, R., Lowick, S. E., Kook, M., Rhodes, E. J., 2015. OSL-
478 thermochronometry of feldspar from the KTB borehole, Germany.

479 Harrison, T. N., Parsons, I., Brown, P. E., 1990. Mineralogical evolution of fayalite-bearing
480 rapakivi granites from the Prins Christians Sund pluton, South Greenland.
481 Mineralogical Magazine 54, 57–66.

482 Hütt, G., Jaek, I., Tchonka, J., 1988. Optical dating: K-feldspars optical response stimulation
483 spectra. Quat. Scr. Rev. 7, 381–385.

484 Huntley, D. J., Godfrey-Smith, D. I., Thewalt, M. L. W., 1985. Optical dating of sediments.
485 Nature 313, 105-107.

486 Ikeya, M., 1993. New Applications of Electron Spin Resonance. World Scientific. ISBN 978-
487 981-4317-21-4.

International Atomic Energy Agency, Analytical Quality Control Services, Seibersdorf (Austria) (1999). IAEA AQCS catalogue for reference materials and intercomparison exercises 1998/1999 (INIS-XA--131). International Atomic Energy Agency (IAEA)

Jain, M., Sohbati, R., Guralnik, B., Murray, A. S., Kook, M., Lapp, T., Prasad, A. K., Thomsen, K. J., Buylaert, J. P., 2015. Kinetics of infrared stimulated luminescence from feldspars. Radiat. Meas. 81, 242–250.

Jain, M., Guralnik, B., Thalbitzer Andersen, M., 2012. Stimulation luminescence emission from localized recombination in randomly distributed defects. J. Phys.: Condens. Matter 24, 1–12.

Jain, M., Ankjærgaard, C., 2011. Towards a non-fading signal in feldspar: Insight into charge transport and tunnelling from time-resolved optically stimulated luminescence. Radiat. Meas. 46, 292–309.

Kars, R. H., Poolton, N.R.J., Jain, M., Ankjærgaard, C., Dorenbos, P., Wallinga, J., 2013. On the trap depth of the IR-sensitive trap in Na- and K-feldspar. Radiat. Meas. 59, 103–113.

King, G. E., Herman, F., Guralnik, B., 2016. Northward migration of the eastern Himalayan syntaxis revealed by OSL thermochronometry. Science 353 (6301), 800–804.

Finch, A. A., Klein, J., 1999. The causes and petrological significance of cathodoluminescence emissions from alkali feldspars. Contrib. Mineral. Petrol. 135, 234-243.

Ito, H., Yamada, R., Tamura, A., Arai, S., Horei, K., Hokada, T., 2013. Earth's youngest exposed granite and its tectonic implications: the 10-0.8 Ma Kurobegawa Granite. Scientific Reports 3: 1306.

509 Kook, M. H., Lapp, T., Murray, A. S., Thiel., C., 2012. A Risø XRF attachement for major
510 element analysis of aliquots of quartz and feldspar separates. UK Luminescence and
511 ESR Meeting, Aberystwyth, September 2012 (abstract), p. 37.

512 Krbetschek, M. R., Götze, J., Dietrich, A., Trautmann, T., 1997. Spectral information from
513 minerals relevant for luminescence dating. Radiat. Meas. 27 (5/6), 695–748.

514 Krbetschek, M. R., Rieser, U., Stolz, W., 1996. Optical dating: Some luminescence properties
515 of natural feldspars. Radiat. Prot. Dos. 66 (1–4), 407–412.

516 Lambert, R., King, G.E., Valla, P.G., Herman, F., In Review. Investigating thermal kinetic
517 processes of feldspar for the application of luminescence thermochronometry. Radiat.
518 Meas.

519 Li, Li, B., Li, S.-H., 2013. The effect of band-tail states on the thermal stability of the infrared
520 stimulated luminescence from K-feldspar. J. Lumin. 136, 5-10.

521 Malins, A. E. R., Poolton, N. R. J., Quinn, F. M., Johnsen, O., Denby, P. M., 2004.
522 Luminescence excitation characteristics of Ca, Na, and K-aluminosilicates (feldspars) in
523 the stimulation range 5–40 eV: determination of the band-gap energies. J. Phys. D:
524 Appl. Phys. 37, 1439–1450.

525 McKeever, S. W. S., Bøtter-Jensen, L., Agersnap Larsen, N., Duller, G. A. T., 1997.
526 Temperature dependence of OSL decay curves: Experimental and theoretical aspects.
527 Radiat. Meas. 27 (2), 161–170.

528 Morthekai, P., Thomas, J., Pandiam, M. S., Balaram, V., Singhvi, A. K., 2012. Variable range
529 hopping mechanism in band-tail states of feldspars: A time-resolved IRSL study. Radiat.
530 Meas. 47, 857–863.

Murray, A. S., Buylaert, J. P., Thomsen, K. J., Jain, M., 2009. The effect of preheating on the IRSL signal from feldspar. Radiat. Meas. 44, 554–559.

Poolton, N.R.J., Kars, R.H., Wallinga, J., Bos, A.J.J., 2009. Direct evidence for the participation of band-tails and excited-state tunneling in the luminescence of irradiated feldspars. J. Phys. Condens. Matter 21, 1-10.

Poolton, N. R. J., Wallinga, J., Murray, A. S., Bulur, E., Bøtter-Jensen, L., 2002a. Electrons in feldspar I: on the wavefunction of electrons trapped at simple lattice defects. Phys. Chem. Minerals 29, 210–216.

Poolton, N. R. J., Ozanyan, K. B., Wallinga, J., Murray, A. S., Bøtter-Jensen, L., 2002b. Electrons in feldspar II: a consideration of the influence of conduction band-tail states on luminescence processes. Phys. Chem. Minerals 29, 217–225.

Poolton, N. R. J., Nicholls, J. E., Bøtter-Jensen, L., Smith, G. M., Riedi, P. C., 2001. Observation of free electron cyclotron resonance in $NaAlSi_3O_8$ feldspar: Direct determination of the effective electron mass. Phys. stat. sol. 225 (2), 467–475.

Prasad, A.K., Lapp, T., Kook, M., Jain, M., 2016. Probing luminescence centres in Na rich feldspar. Radiat. Meas. 90, 292-297.

Prasad, A. K., Poolton, N. R. J., Kook, M., Jain, M., 2017. Optical dating in a new light: A direct, non-destructive probe of trapped electrons. Scientific Reports 7, 1–15.

Prasad, A. K., Jain, M., 2018. Breakdown of Kasha´s Rule in a Ubiquitous, Naturally Occuring, Wide Bandgap Aluminosilicate (Feldspar). Scientific Reports 8, 1–12.

Riedesel, S., Brill, D., Roberts, H.M., Duller, G.A.T., Garrett, E., Zander, A.M., King, G.E., Tamura, T., Burow, C., Cunningham, A., Seeliger, M., De Batist, M., Heyvaert, V.M.A., Fujiwara, O., Brückner, H. and the QuakeRecNankai Team, 2018. Single-grain

554 luminescence chronology of historical extreme-wave event deposits recorded in a
555 coastal lowlans, Pacific coast of central Japan. Quat. Geochronol. 45, 37–49.

556 Sanderson, D.C.W., Clark, R.J., 1994. Pulsed photostimulated luminescence of alkali feldspars.
557 Radiat. Meas. 23, 633–639.

558 Short, M. A. (2004). Determining the possible lattice sites of two unknown defects in
559 orthoclase from the polarization effects in their optical transitions. Journal of Physics:
560 Condensed Matter, 16(41), 7405.

561 Spooner, N. A., 1994. The anomalous fading of infrared-stimulated luminescence from
562 feldspars. Radiat. Meas. 23, 625–632.

563 Stickertsson, K., 1985. The thermoluminescence of potassium feldspars – glow curve
564 characteristics and initial rise measurements. Nucl. Tracks 10, 613–617.

565 Thiel, C., Buylaert, J.-P., Murray, A., Terhorst, B., Hofer, I., Tsukamoto, S., Frechen, M., 2011.
566 Luminescence dating of the Stratzig loess profile (Austria) – Testing the potential of an
567 elevated temperature post-IR IRSL protocol. Quat. Int. 234, 23–31.

568 Thomsen, K. J., Murray, A. S., Jain, M., Bøtter-Jensen, L. 2008: Laboratory fading rates of
569 various luminescence signals from feldspar-rich sediment extracts. Radiat. Meas. 43,
570 1474– 1486.

571 Tsukamoto, S., Jain, M., Murray, A., Thiel, C., Schmidt, E., Wacha, L., Dohrmann, R., Frechen,
572 M., 2012. A comparative study of the luminescence characteristics of polymineral fine
573 grains and coarse-grained K- and Na-rich feldspars. Radiat. Meas. 47, 903–908.

574 Wintle, A. G., 1973. Anomalous fading of thermoluminescence in mineral samples. Nature
575 245, 143–144.

576 Yukihara, E.G., Coleman, A.C., Biswas, R.H., Lambert, R., Herman, F., King, G.E., In Press.
577 Thermoluminescence Analysis for Particle Temperature Sensing and
578 Thermochronometry: Principles and Fundamental Challenges. Radiation
579 Measurements.

580

581

582 **Figure captions**

583

584 **Fig. 1:** Energy band model with density of states, recombination processes and energy
585 transitions of the principal trap in feldspar. A) Distribution of the density of states, Gaussian
586 distributions correspond to different energy states (e.g. the ground state and excited state
587 of the IRSL (principal) trap in feldspar). While the density of sub-conduction band-tail states
588 are thought to be exponentially distributed with energy below the conduction band edge,
589 energy states in the conduction band follow a parabolic shape (modified from Poolton et al.,
590 2002b; Jain & Ankjærgaard, 2011). The full sub-conduction band-tail width (i.e. the Urbach
591 width) is referred to as E_u (as they are also called Urbach tail), and may extend below the
592 ground state of the principal trap, whereas ΔE defines the band-tail states accessible form
593 the ground state of the defect. B) Possible transitions from the ground state of the IRSL trap
594 (modified from Jain & Ankjærgaard, 2011). a) Thermal excitation. b) Optical excitation by
595 different wavelengths; whereas blue light stimulation allows immediate transition into the
596 conduction band, green light results in a sub-conduction band transition and IR stimulation
597 excites the electron to the excited state. c) Recombination through the conduction band. d)
598 Recombination through the band-tail states. When the electron has been excited to the
599 excited state of the trap by IR stimulation, phonon-assisted diffusion (PAD) allows transition
600 through the band-tail states. e) Athermal signal loss due to quantum mechanical tunnelling
601 from the ground state of the trap. f) Retrapping, which may result in a photon with the same
602 energy as the absorbed photon.

603

604 **Fig. 2:** Feldspar ternary of chemical composition and origin map for samples in this study.

605

Fig. 3: Example excitation spectra: A) Rising continuum of F1, measured at 7 and 300 K; B) Excitation spectra of Cleavelandite, KRG-16-112 and MBT-I-2430. These spectra are representative for the range of sample brightness and the shape of the IR resonance peak and non-resonant rising continuum. In contrast to the other samples investigated, MBT-I-2430 also shows a peak centred at ~2.10 eV superimposed on the rising continuum.

Fig. 4: Excitation spectrum of KTB-383-C showing model fits. The IR resonance peak was fitted with a single Gaussian distribution [eq. 2] and the rising continuum was fitted with equation 1 (Bøtter-Jensen et al., 2003) to estimate trap depth and equation 3 (Poolton et al., 2009) to obtain an estimate of the band-tail width accessible from the ground state of the trap (ΔE). Each part of the excitation spectrum was fitted separately.

Fig. 5: Photoluminescence emission spectra of the excitation-energy-dependent emission (EDE) and the full band-tail width (E_u) calculation for Cleavelandite. A) EDE spectra. B) Normalised EDE spectra. C) Exponential relationship between the integrated area under the emission spectrum and the corresponding excitation energy. The inverse of the slope (1/e) gives E_u.

Fig. 6: Comparison of band-tail states accessible from the ground state of the trap (ΔE) and the full band-tail width (E_u) calculated from fitting the rising continuum with eq. 3 and by using EDE respectively. The dashed line indicates the 1:1 relationship.

Fig. 7: Summary of trap depth, band-tail width and position of the IR resonance peak, obtained from optical measurements. Results of this study are compared to published

630 research. Baril & Huntley (2003) investigated 19 samples, since all their samples show a main
631 IR-resonance at 1.44–1.45 eV, just a single point represents their data.

632

633

634 **Table 1**: List of samples with chemical composition (determined using the Risø XRF OSL/TL
635 reader attachment, Kook et al., 2012) and geological origin.

ID	Type[1]	Origin	Chemical composition[2] (FS %[3])			Quartz amount (%)	Geological age	
			Or	Ab	An			
NB139	Bedrock	Migmatitic gneiss, Namche Barwa, Nepal	89.3	9.4	1.4	4.2	Proterozoic (Burg et al., 1997)	
NB120	Bedrock	Migmatitic gneiss, Namche Barwa, Nepal	86.2	11.0	2.9	5.0	Proterozoic (Burg et al., 1997)	
MBT-I-2430	Bedrock	Calc-alkaline granite,Mont Blanc Tunnel, Italy	86.7	12.0	1.3	4.2	~300 Ma (Bussy et al., 1989; Bussy and Von Raumer, 1993)	
MBT-F-5704	Bedrock	Calc-alkaline granite, Mont Blanc Tunnel, France	76.3	22.5	1.2	4.6	~300 Ma (Bussy et al., 1989; Bussy and Von Raumer, 1993)	
KRG-16-06	Bedrock	Kurobegawa granite, Japanese Alps, Japan	79.4	17.3	3.2	3.1	<10 Ma (Ito et al., 2013)	
KGR-16-112	Bedrock	Kurobegawa granite, Japanese Alps, Japan	75.2	21.3	3.5	3.4	<10 Ma (Ito et al., 2013)	
R1-11A	Museum	Rapakivi Granite, South Greenland	68.0	22.0	10.0		c. 1750 Ma (Finch and Klein, 1999)	Harri
F1	IAEA AQCS Reference Feldspar		61.3	33.4	5.4	0.3	NA	Sa
JSH1-13	Sediment	Shirasuka Lowlands, Japan	50.4	37.6	12.1	38.1	NA	Ried
HAM-5	Sediment	Lake Hamana, Japan	64.9	31.1	4.0	19.3	NA	
KTB-383-C	Bedrock	KTB borehole, Germany	18.2	67.6	14.4	52.8		Gura
Cleavelandite	Museum	Pegmatite, Golonca District, Minas Gerais, Brazil	0.5	99.3	0.2	3.9	650-450 Ma (Cassedanne and Roditi, 1996)	
DK4	Museum	Klokken intrusion, Sout Greenland	5.0	36.0	59.0		1.18 Ma	

636
637 Notes:
638 [1] Museum specimen are single crystals, the IAEA reference feldspar, feldspars extracted from bedrock and
639 sediment samples were mounted as coarse multiple-grain aliquots
640 [2] Determined by XRF measurements
641 [3] Assuming 100 % feldspar
642 .

643

Table 2: Optical kinetics of feldspar samples investigated in this study. The reported uncertainties account only for the fitting, no uncertainties resulting from the instrumentation are added.

Sample[1]	Optical trap depth (eV)[2]	Excited state (IR resonance peak)[3]			Band-tail width (ΔE, fitting using eq. 3)		Band-tail width (E_u, eV)
		Mode (eV)	Standard deviation (sigma, eV)	FWHM	ΔE (eV)	Fitted excitation energy range (eV)	
NB139	2.03 ± 0.02	1.46	0.09	0.21	0.39 ± 0.01	1.80 – 2.48	0.37 ± 0.01
NB120	2.03 ± 0.04	1.45	0.11	0.26	0.47 ± 0.02	1.80 – 2.48	0.42 ± 0.01
MBT-I-2430	2.15 ± 0.01	1.45	0.07	0.16	0.22 ± 0.01	2.22 – 2.48	0.32 ± 0.01
MBT-F-5704	2.05 ± 0.01	1.44	0.08	0.19	0.31 ± 0.01	1.80 – 2.48	0.30 ± 0.03
KRG-16-06	NA	1.44	0.14	0.33	0.46 ± 0.03	1.80 – 2.48	0.42 ± 0.01
KRG-16-112	NA	1.41	0.16	0.38	NA	NA	0.45 ± 0.01
R1-11A	2.02 ± 0.03	1.43	0.12	0.28	0.38 ± 0.01	1.80 – 2.48	No shift
F1	NA	1.45	0.10	0.24	0.29 ± 0.01	1.80 – 2.48	0.48 ± 0.03
F1 (7 K)	2.10 ± 0.02	no peak	no peak	no peak	0.21 ± 0.00	1.80 – 2.48	no peak shift
JSH1-13	2.01 ± 0.01	1.43	0.10	0.24	0.36 ± 0.01	1.80 – 2.48	0.50 ± 0.01
HAM-5	2.03 ± 0.01	1.43	0.10	0.24	0.31 ± 0.00	1.80 – 2.48	0.42 ± 0.01
KTB-383-C	2.04 ± 0.01	1.43	0.09	0.21	0.30 ± 0.00	1.80 – 2.48	0.81 ± 0.03
Cleavelandite	1.99 ± 0.01	1.45	0.10	0.24	0.34 ± 0.01	1.80 – 2.48	0.33 ± 0.00
DK4	NA	1.41	0.17	0.40	NA	NA	0.26 ± 0.02

Notes:
[1] Samples are sorted from high to low potassium content, DK4 is a plagioclase.
[2] Excitation energy range used for fitting with equation 1: 2.30 – 2.48 eV
[3] The parameters refer to the fitted Gaussian distribution (eq. 2), not to the peak itself.

Supplementary Material

Fig. S-1: Excitation spectra fitted using eq. 1 (Bøtter-Jensen et al., 2003) to determine trap-depth (E_t) for F1, which was measured at 7 K. The solid line shows the fit and the dashed line the extrapolated curve. The intersect of the dashed curve with the x-axis gives the trap depth.

Fig. S-2: Excitation spectra fitted using eq. 1 (Bøtter-Jensen et al., 2003) to determine trap-depth (E_t) for samples NB139, NB120, MBT-I-2430, MBT-F-5704, R1-11A and JSH1-13, all measured at 300 K. The solid line shows the fit and the dashed line the extrapolated curve. The intersect of the dashed curve with the x-axis gives the trap depth.

Fig. S-3: Excitation spectra fitted using eq. 1 (Bøtter-Jensen et al., 2003) to determine trap-depth (E_t) for samples HAM-5, KTB-383-C and Cleavelandite, all measured at 300 K. The solid line shows the fit and the dashed line the extrapolated curve. The intersect of the dashed curve with the x-axis gives the trap depth.

Fig. S-4: Excitation spectra showing the fit of the IR resonance peak of samples NB139, NB120, MBT-I-2430, MBT-F-5704, KGR-16-06, KRG-16-112, R1-11A and F1 with a single Gaussian distribution [eq. 2].

Fig. S-5: Excitation spectra showing the fit of the IR resonance peak of samples JSH1-13, HAM-5, KTB-383-C, Cleavelandite and DK4 with a single Gaussian distribution [eq. 2].

685 **Fig. S-6:** Excitation spectra of samples NB139, NB120, MBT-I-2430, MBT-F-5704, KRG-16-06,
686 KRG-16-112 and R1-11A fitted with equation 3 (Poolton et al., 2009) to obtain the width of
687 the band-tail accessible from the ground state of the trap (ΔE).
688
689 **Fig. S-7:** Excitation spectra of samples F1 (300 K and 7 K), JHS1-13, HAM-5, KTB-383-C,
690 Cleavelandite and DK4 fitted with equation 3 (Poolton et al., 2009) to obtain the width of the
691 band-tail accessible from the ground state of the trap (ΔE).
692
693 **Fig. S-8:** Exponential relationship of the integrated area under the PL peak and the
694 corresponding excitation energy of samples NB139, NB120, MBT-I-2430, MBT-F-5704, KRG-
695 16-06 and KRG-16-112. The inverse of the slope gives the band-tail width (E_u).
696
697 **Fig. S-9:** Exponential relationship of the integrated area under the PL peak and the
698 corresponding excitation energy of samples F1, JHS1-13, HAM-5, KTB-383-C, Cleavelandite
699 and DK4. The inverse of the slope gives the band-tail width (E_u).
700

701 **Table S-1:** Trap depth estimates using equation 1 (Bøtter-Jensen et al., 2003) for different

702 integration ranges.

703

	Optical trap depth (eV)					
Sample[1]	**2.10–2.48 eV**	**2.15–2.48 eV**	**2.20–2.48 eV**	**2.25–2.48 eV**	**2.30–2.48 eV**	**2.35–2.48 eV**
NB139	1.86 ± 0.02	1.90 ± 0.02	1.94 ± 0.02	1.97 ± 0.02	2.03 ± 0.2	2.06 ± 0.03
NB120	1.84 ± 0.03	1.89 ± 0.03	1.95 ± 0.03	2.01 ± 0.03	2.03 ± 0.04	2.09 ± 0.05
MBT-I-2430	1.95 ± 0.02	2.01 ± 0.02	2.07 ± 0.01	2.11 ± 0.03	2.15 ± 0.01	2.19 ± 0.01
MBT-F-5704	1.93 ± 0.01	1.97 ± 0.01	2.00 ± 0.01	2.03 ± 0.01	2.05 ± 0.01	2.07 ± 0.02
R1-11A	1.88 ± 0.02	1.91 ± 0.02	1.96 ± 0.02	1.98 ± 0.03	2.02 ± 0.03	2.06 ± 0.05
F1[2]	2.02 ± 0.01	2.05 ± 0.01	2.06 ± 0.01	2.08 ± 0.01	2.10 ± 0.02	2.11 ± 0.03
JSH1-13	1.88 ± 0.01	1.90 ± 0.01	1.94 ± 0.01	1.97 ± 0.01	2.01 ± 0.01	2.02 ± 0.01
HAM-5	1.92 ± 0.01	1.95 ± 0.01	1.98 ± 0.01	2.01 ± 0.01	2.03 ± 0.01	2.04 ± 0.01
KTB-383-C	1.93 ± 0.01	1.96 ± 0.01	1.99 ± 0.01	2.02 ± 0.01	2.04 ± 0.01	2.05 ± 0.01
Cleavelandite	1.88 ± 0.01	1.91 ± 0.01	1.94 ± 0.01	1.97 ± 0.01	1.99 ± 0.01	2.01 ± 0.01

704

705

706 Notes:
707 [1] Samples are sorted from high to low K-content.
708 [2] F1 was measured at 7 K.

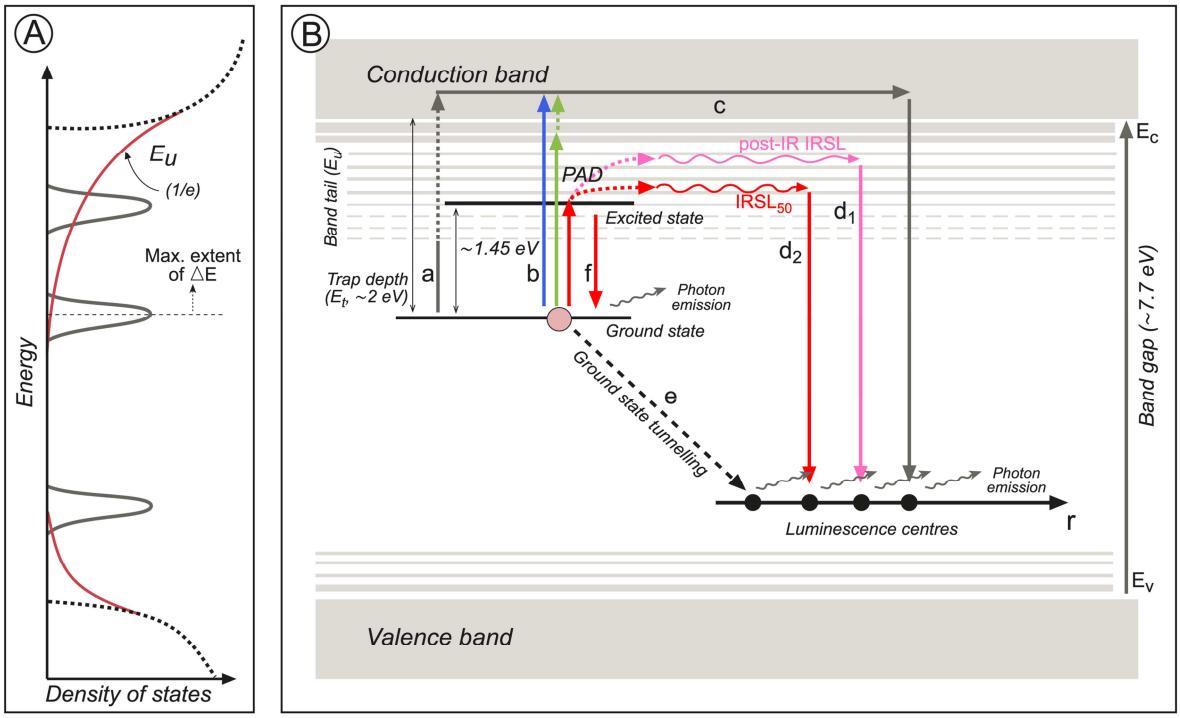

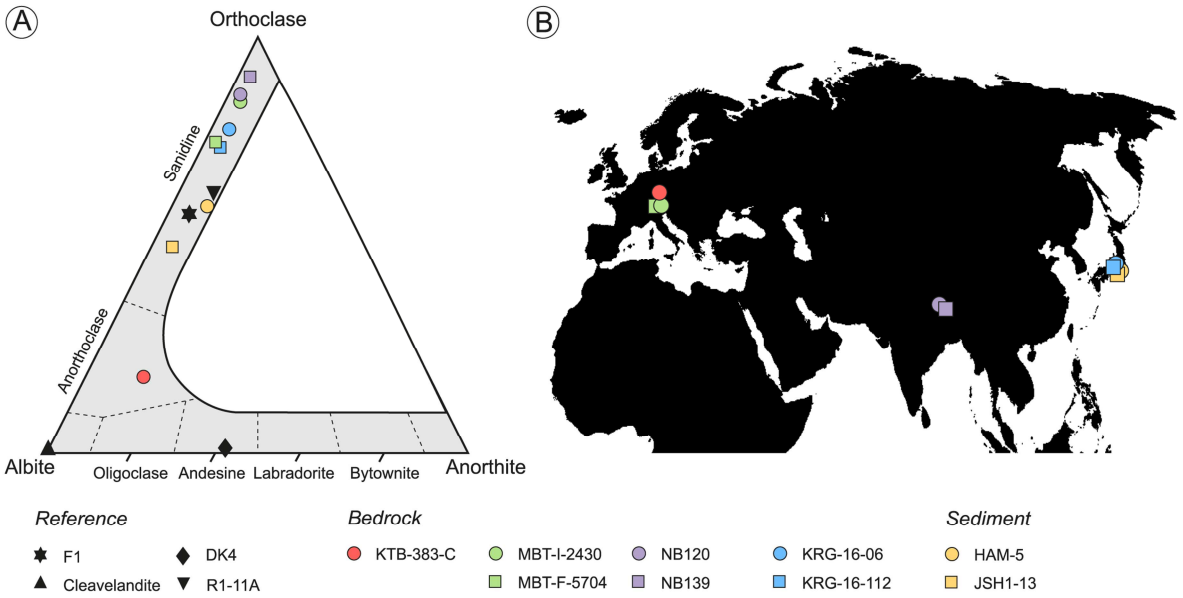

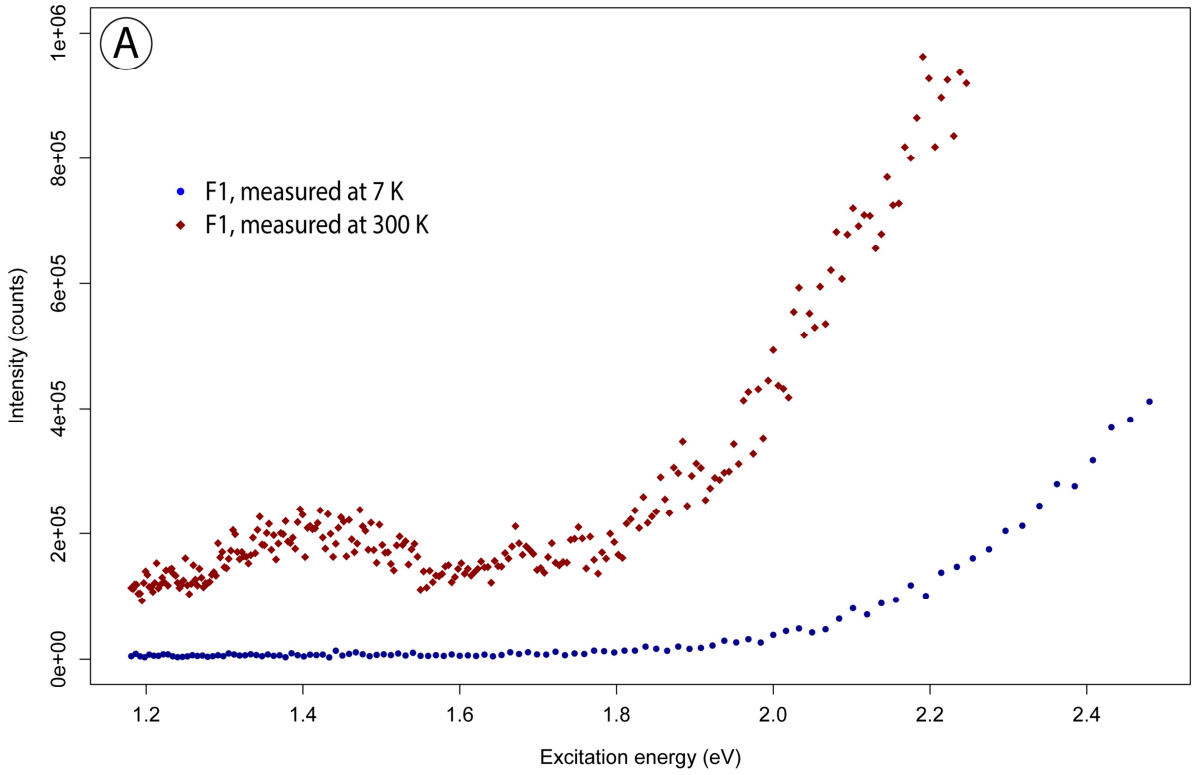
A
F1, measured at 7 K
F1, measured at 300 K
Intensity (counts)
0e+00
2e+05
4e+05
6e+05
8e+05
1e+06
1.2
1.4
1.6
1.8
2.0
2.2
2.4
Excitation energy (eV)

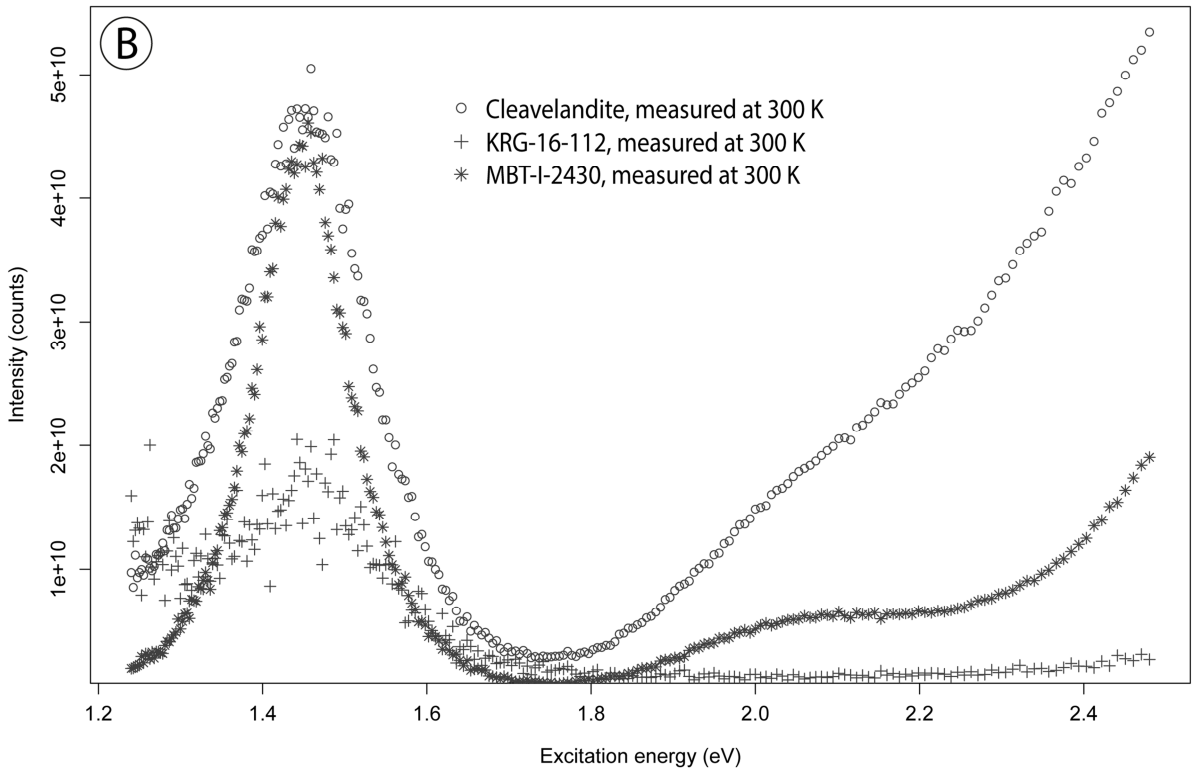
B
Cleavelandite, measured at 300 K
KRG-16-112, measured at 300 K
MBT-I-2430, measured at 300 K
Intensity (counts)
1e+10
2e+10
3e+10
4e+10
5e+10
1.2
1.4
1.6
1.8
2.0
2.2
2.4
Excitation energy (eV)

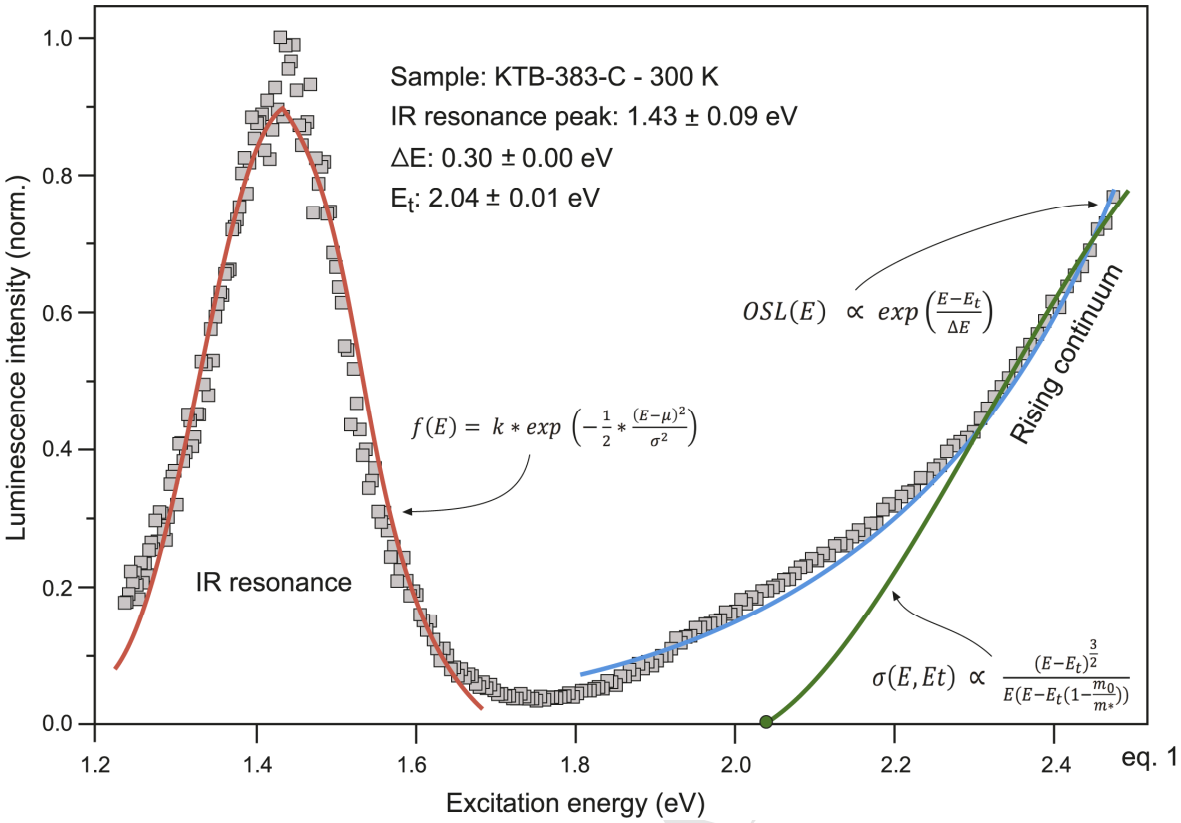

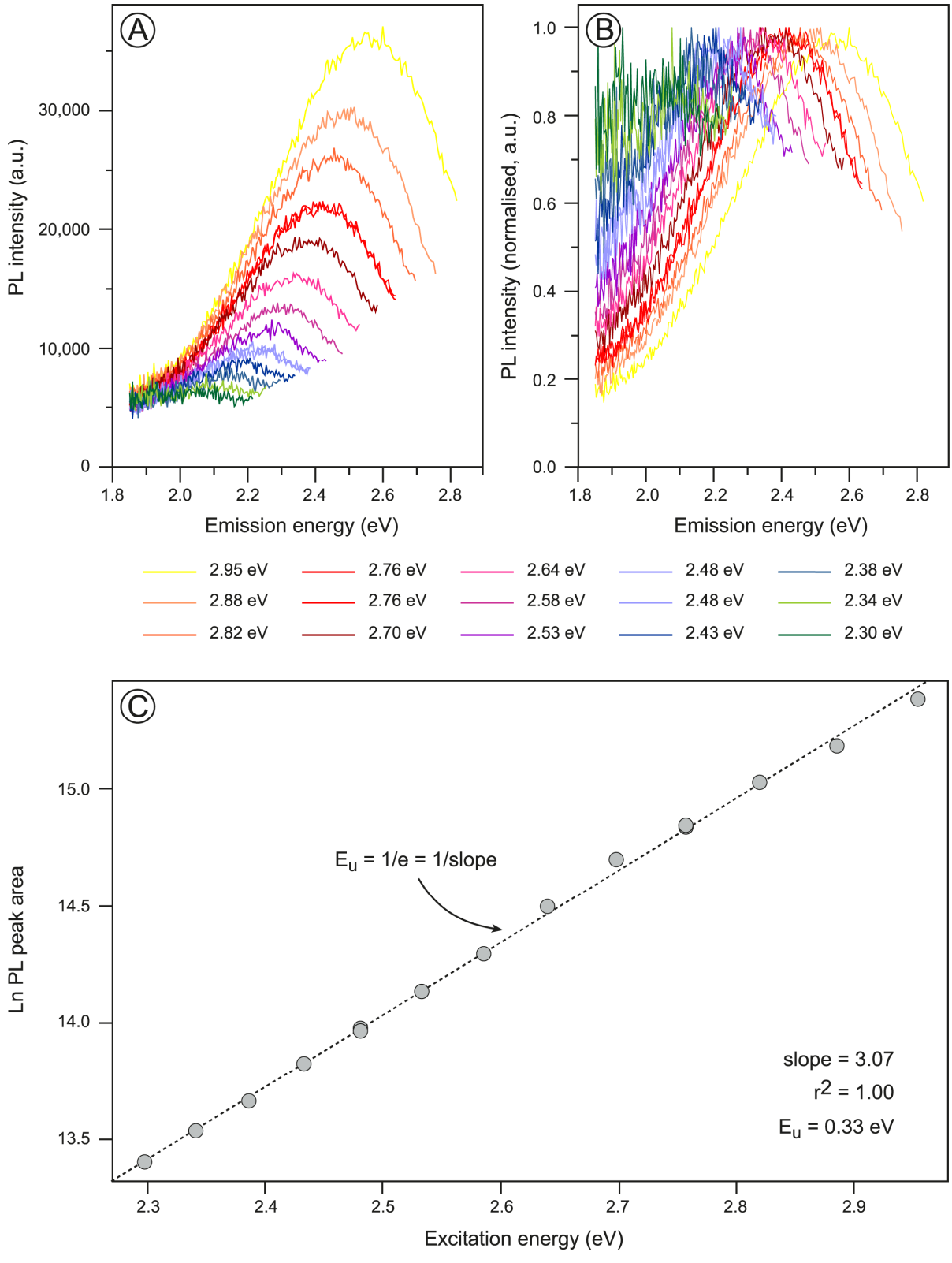
A
B
C
PL intensity (a.u.)
PL intensity (normalised, a.u.)
Emission energy (eV)
Emission energy (eV)
2.95 eV
2.88 eV
2.82 eV
2.76 eV
2.76 eV
2.70 eV
2.64 eV
2.58 eV
2.53 eV
2.48 eV
2.48 eV
2.43 eV
2.38 eV
2.34 eV
2.30 eV
Ln PL peak area
Excitation energy (eV)
E_u = 1/e = 1/slope
slope = 3.07
r2 = 1.00
E_u = 0.33 eV

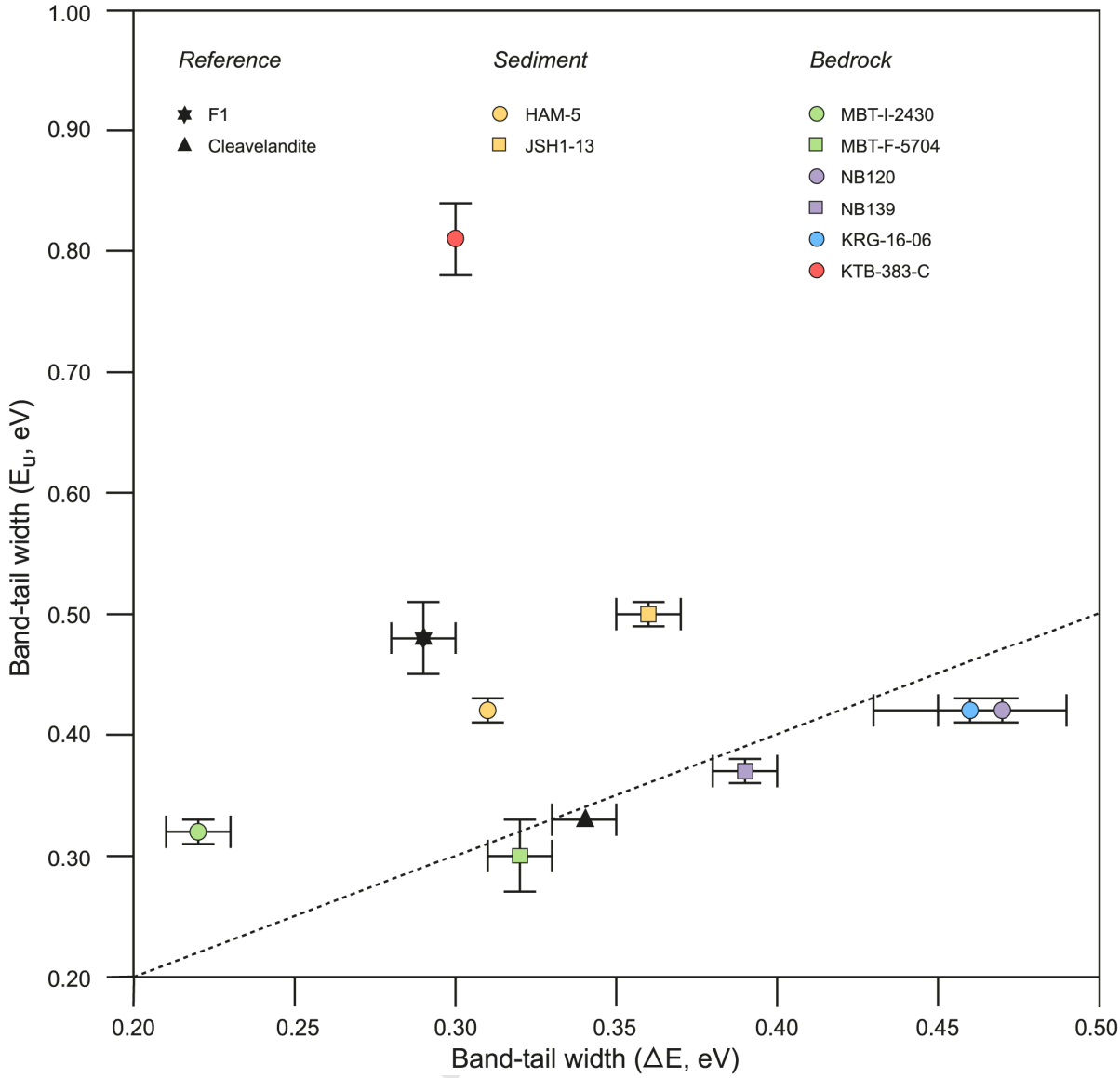

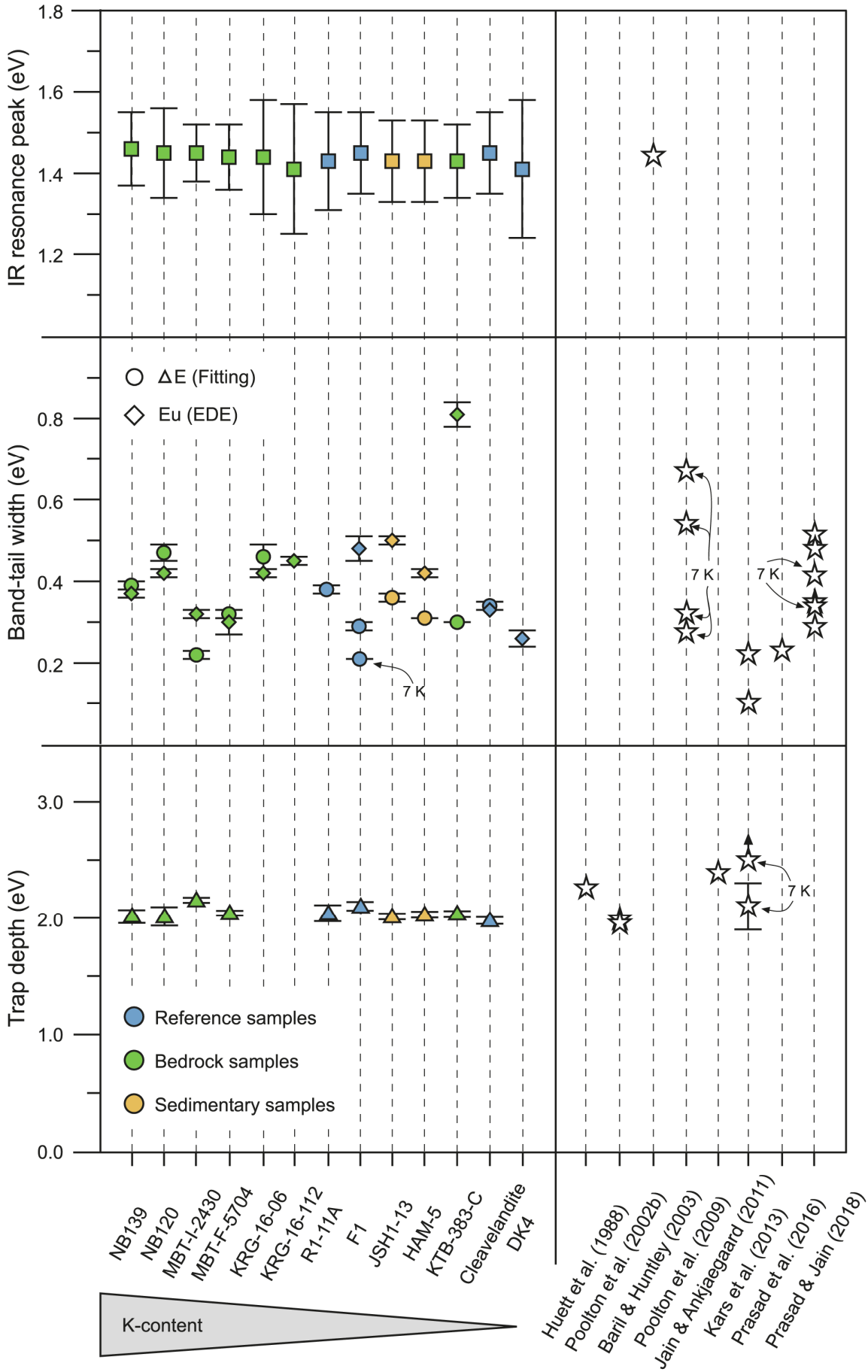
IR resonance peak (eV)
1.8
1.6
1.4
1.2
Band-tail width (eV)
ΔE (Fitting)
Eu (EDE)
0.8
0.6
0.4
0.2
7 K
7 K
7 K
Trap depth (eV)
3.0
2.0
1.0
0.0
7 K
Reference samples
Bedrock samples
Sedimentary samples
NB139
NB120
MBT-I-2430
MBT-F-5704
KRG-16-06
KRG-16-112
R1-11A
F1
JSH1-13
HAM-5
KTB-383-C
Cleavelandite
DK4
Huett et al. (1988)
Poolton et al. (2002b)
Baril & Huntley (2003)
Poolton et al. (2009)
Jain & Ankjaegaard (2011)
Kars et al. (2013)
Prasad et al. (2016)
Prasad & Jain (2018)
K-content

Highlights

- Thirteen chemically different feldspars characterised
- Ground and excited state energies of the trap invariant with chemical composition
- Sub-conduction band-tail states width more variable between feldspars